Z. Kristallogr. **219** (2004) 370–375

Electronic structure and bonding in antimony and its high pressure phases

Alim Ormeci* and Helge Rosner

Max-Planck-Institut für Chemische Physik fester Stoffe, Nöthnitzer Str. 40, 03187 Dresden, Germany

Received November 6, 2003; accepted January 19, 2004

Electronic structure / Electron Localization Function / Incommensurate host-guest structure / High pressure / Antimony

Abstract. The effects of pressure on the electronic structure and on the bonding properties of Sb are studied by first-principles electronic structure methods. A commensurate approximate structure is used in the calculations for the modulated incommensurate Sb-II phase. It is found that the overlap of *s* and *p* bands increases with increasing pressure resulting in pressure-induced metallization of Sb. Analyses based on the electron localization function show that there is no chemical bond between the chain atoms of a previously suggested Sb-II structure. The high total energy of this structure with respect to other structures considered is a result of the absence of this binding.

Introduction

The major improvements of the last decade in the high pressure experimental techniques have resulted in many high-pressure crystal structures of elemental solids being successfully solved [1–3]. Some more complex atomic patterns have been found, such as arrangements with incommensurate host-guest sublattices, or with unit cells of more than 50 atoms [4–7]. In parallel to these experimental achievements first-principles electronic structure methods have also shown considerable progress regarding accuracy and the ability of studying crystalline material with a larger number of atoms in the unit cell. In general excellent agreement between experimental and theoretical results has been obtained in the study of the high pressure phases of elemental solids [8–14].

A recent example is the Sb-II phase of Sb [15]. Sb crystallizes in a rhombohedral structure called A7 at pressures up to 8.5 GPa. The phase that follows is designated as Sb-II. At a pressure of about 28 GPa Sb-II converts into the cubic body centered (BCC) structure [16]. The structure of the Sb-II modification has been a matter of controversy for a long time [17]. A tetragonal model with space group $P4/n$ containing 10 atoms per cell was suggested in 1990 [18]. In this model Sb atoms occupy two inequivalent Wyckoff sites; one set of sites forms a three-dimensional framework, and the other forms chains running through the provided channels. In what follows we will refer to the atoms forming the framework (chain) as *host* (*guest*) atoms. A later investigation of Sb-II found a more elaborate host-guest structure [4]: both the host and the guest sublattices are body centered tetragonal with the same *a* lattice parameter, but their *c* lattice parameters are incommensurate with respect to each other. However, even this complicated model did not account for a few weak reflections. A fully satisfactory solution was obtained when, in addition to the already incommensurate host-guest sublattices, first order modulation waves in both sublattices were taken into account [15]. However, in the first-principles electronic structure calculations for the Sb-II phase a commensurate structure model approximating the modulated composite was used [13, 15]. The total-energy calculations correctly reproduced the order of structural transitions: A7 → *Approximant* → BCC. The first model based on $P4/n$ symmetry was found to be about 80 meV per atom higher in total energy than the approximant [15]. The calculated transition pressures, fractional volume changes at the transition and the pressure – volume curves were also in perfect agreement with their experimental counterparts [13, 15].

In this study we investigate the effects of pressure on the electronic structure and on the bonding properties of Sb. For this purpose we used two different all-electron full-potential methods, namely full-potential linear muffin-tin-orbital method (FP-LMTO) [19] and full-potential local orbital method (FPLO) [20]. Further, we employed the tight-binding linear muffin-tin-orbital method within the atomic-sphere approximation (TB-LMTO-ASA) [21, 22]. The latter was needed for computing the electron localization function (ELF) [23, 24]. Electronic structure calculations were performed on the observed structures, A7, approximant (standing for the modulated incommensurate Sb-II phase) and BCC, together with the $P4/n$ structure (which will be referred to as tetragonal primitive or TP) previously proposed [18].

Description of the structural models

Since the Sb-II modification is a modulated incommensurate structure it has to be approximated by a commensu-

* Correspondence author (e-mail: ormeci@cpfs.mpg.de)

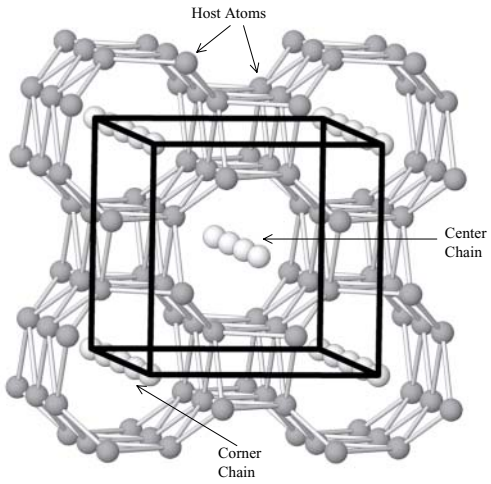

Fig. 1. The crystal structure of Sb-II as modeled by the approximant. Host (guest) atoms are represented by darker (lighter) circles. The linear chains run along the z-axis.

rate model with conventional 3D translational symmetry in order to use standard computer codes for the calculations. If the c lattice parameter of the host structure is denoted by c_h, and that of the guest structure by c_g, then the ratio c_h/c_g is found to vary by less than 0.4% within the stability range of Sb-II [15]. The value of this ratio at 12 GPa is 1.311 and therefore a commensurate approximant with a ratio of $^4/_3$ is an optimal choice balancing a managable small number of atoms in the supercell and similarity of model and real structure.

The unit cell of such an approximant contains 24 host and 8 guest atoms. The crystal structure is shown in Fig. 1. There is a free parameter in the construction of the approximant. If the $z = 0$ layer is taken to be a guest layer, then the z coordinate of the first host layer, due to the incommensurate nature of the Sb-II structure, can be any real number between 0 and $^1/_6$ (in terms of the c lattice parameter of the approximant). Our choice for this offset is such that the guest and host layers coincide at $z = {}^1/_4$ and $z = {}^3/_4$ [25].

The range of lattice parameters for all the structures considered in this study are listed in Table 1. The nearest guest-guest distance occurs along chains and corresponds to $d_{GG} = 0.366a$ in terms of the a lattice parameter common to both sublattices. The shortest host-host distances are $d_{HH} = 0.357a$ and $0.399a$. These distances are independent of the choice of the offset. For the nearest host-guest neighbors, there are three types of short contacts whose bond lengths depend on the offset. The shortest host-guest distance is between the coplanar host and guest atoms and is given by $d_{HG} = 0.377a$. This is the lowest possible value for the host-guest distances. The other two distances in the approximant that we use, are: $d_{HG} = 0.382a$ and $0.396a$. Taking only these kinds of neighbors into account we arrive at the following coordination numbers (CN): either 6 or 10 for guest atoms depending on their location, and 7 or 8 for host atoms [15]. The 7-coordinated host atoms are those that are coplanar with the guest atoms. Because of this, their distance to the neighboring guest layers is a maximum and their next-nearest guest-atom neighbors lie at a distance of $0.419a$, which sets the upper limit for this type of neighbors. In the actual Sb-II structure these exactly coplanar layers will be replaced by layers with arbitrarily small interlayer spacings. However, these variations do not alter the result that CN = 7 for such host atoms. The host atoms whose layers are not too close to the guest layers have two near guest atoms.

Table 1. The lattice parameters of the structures used in the calculations are listed below in units of Å. The c/a ratios are 2.610, 1.464 and 0.484 for A7, approximant and TP, respectively.

Phase	A7	Sb-II	BCC
Volume (Å^3)	31.000–25.777	24.018–22.348	21.776–18.770
A7	4.350–4.090	3.995–3.900	3.867–3.680
Approximant	8.783–8.259	8.067–7.875	7.807–7.430
TP	8.619–8.104	7.916–7.728	7.661–7.291
BCC	3.958–3.722	3.635–3.549	3.518–3.348

Among the distances listed above the shortest ones occur between host-host and guest-guest neighbors. In the stability range of Sb-II these distances correspond to 2.814–2.882 Å and 2.883–2.953 Å for host-host and guest-guest distances, respectively. For comparison the nearest neighbor distance in the A7 structure varies between 2.868–2.940 Å within its own stability range. Thus, the shortest interatomic distances do not differ much between the A7 structure and the approximant. On the BCC side, the nearest-neighbor distance is quite longer due to the increased $8 + 6$ coordination. The volume at which BCC phase becomes stable according to first-principles calculations [15], 21.776 Å^3, gives 3.047 Å as the nearest-neighbor distance.

It is instructive to compare the structural properties of the approximant with those of the $P4/n$ model of Ref. [18]. As indicated in Introduction total energy calculations find the TP structure above the approximant by about 80 meV/atom over the whole volume range of interest [15]. Given the fact that this structure was accounting for the X-ray diffraction data available by 1990 satisfactorily, this energy difference appears to be quite large. Therefore, we would like to see in what aspects structural differences contribute to this remarkable total energy difference. The a lattice parameters are similar in both structures, and the difference between the c lattice parameter of the approximant, c^{Apprx}, and the triple of TP, $3c^{\mathrm{TP}}$, is just 0.8%. Hence, we can form a supercell of the TP structure with 30 atoms in the primitive tetragonal unit cell. Let's denote this arrangement as TP30. We immediately realize that despite similar volumes the approximant has 32 atoms whereas TP30 has two guest atoms less per unit cell. As a consequence the nearest-neighbor distance within the chain of guest atoms in TP30 is longer by $^1/_3$. Since d_{GG} in the approximant is within the bonding range, we expect that in TP30 (and in the TP structure, equivalently) the contribution to binding originating from the guest-guest interactions is missing. The lack of this component easily accounts for the large total energy difference. Regarding the host, the atomic positions are rather similar in both structures and therefore also the contribution to total energy.

Theoretical aspects

The local density approximation (LDA) [26] to the density functional theory [27] was employed in all the calculations reported here. The technical details of the full potential methods used in this study can be found in our earlier work [15]. In the TB-LMTO-ASA calculations the combined correction term was included and empty spheres were inserted in order to keep the amount of total atomic volume overlap at a reasonable level. The positions and the radii of the empty spheres were determined automatically by the code [22].

The TB-LMTO-ASA method is one of the few computational schemes for which ELF has been implemented. The ELF has the form [23]

$$\mathrm{ELF}(\vec{r}) = \frac{1}{1+\chi^2(\vec{r})}, \quad \text{where} \quad \chi(\vec{r}) = t_P(\vec{r})/t_h(\vec{r})\,.$$

According to Savin *et al.* [24] $t_P(\vec{r})$ is the Pauli kinetic energy density and $t_h(\vec{r})$ is the kinetic energy density of a uniform electron gas whose electron density is that of the actual system at that point, $\rho(\vec{r})$. The ELF, by definition, varies between 0 and 1. High ELF values mean that the probability of finding a like spin electron around the reference electron is low. Topological analysis of ELF can be used to extract information on the bonding properties of molecules and crystals [28–31]. In this study the basins, ELF attractors, and number of electrons contained in basins are determined by the program Basin [32].

Results and discussion

When an elemental solid is subjected to increasing pressure the electronic configuration of its atoms can change dramatically. Prime examples of this category are provided by the alkali metals. On the other hand, for elements with an *sp* valence shell, the effects are more subtle. Here, the basic effects of pressure are (i) increased bandwidths, (ii) enhanced overlap of *s* and *p* bands, and (iii) increased

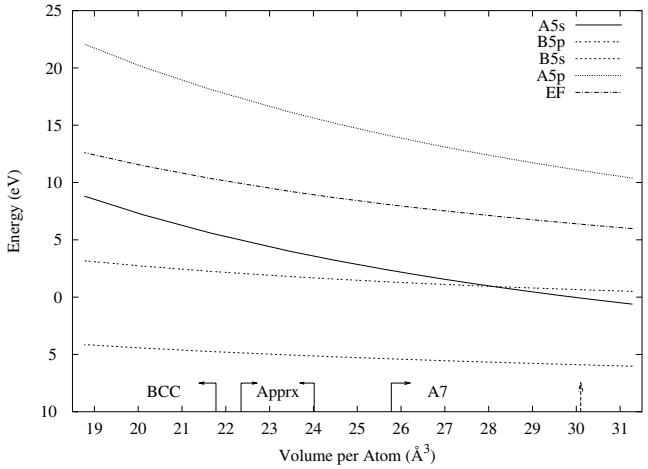

Fig. 2. Variation of Fermi energy, top- and bottom-of-the-band values with atomic volume. The regions of stability for each structure are indicated by full arrows and labelled appropriately. The ambient pressure volume is shown by a dashed-arrow.

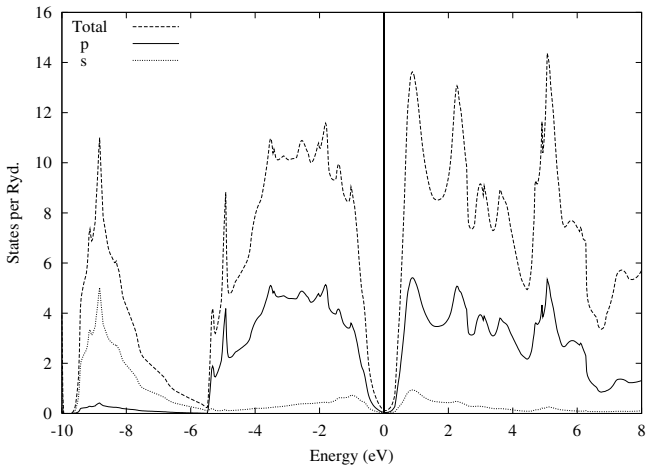

Fig. 3. Density of states computed in the A7 structure at ambient pressure volume.

number of nearest neighbors. As a result, in elemental solids of this category semiconductor (or semimetal) to metal transitions are observed. For example, the calculated density of states for the Si-VI structure shows a nearly free-electron-like feature [9]. Being a member of Group 15, Sb also falls into this category.

By using the Wigner-Seitz rule [33] top- and bottom-of-the-band values for the 5*s* and 5*p* states are computed for all structures considered here. At a given volume these values are within ~ 0.7 eV of each other in all structures. Thus, in Fig. 2 we show the variation of these quantities and the Fermi energy, E_F, as a function of atomic volume as computed for the BCC structure. First, we observe that the bandwidths, defined as the difference between the top and the bottom of the bands, increases with raising pressures as mentioned above. Secondly, at volumes larger than $\sim$28 Å^3, the bottom of the 5*p* band, B5p, is seen to lie above the top of the 5*s* band, A5s. This volume 28 Å^3 corresponds to a pressure of 2.9 GPa as computed from the equation-of-state of the A7 structure. Hence according to this approximate scheme [34], for pressures less than ~ 2.9 GPa *s* and *p* states do not overlap in energy. However, the experimental volume at ambient conditions (30.1 Å^3, indicated by a dashed-arrow in Fig. 2) is obviously in this region, and the density of states (DoS) computed for Sb at ambient pressure (see Fig. 3) shows that there is actually a small amount of *s*-*p* overlap. In the A7 structure the three *p* electrons of an Sb atom form covalent bonds with the *p* electrons of the three nearest neighbors. The three states due to the bonding *p*-*p* orbitals are fully occupied, whereas the antibonding *p*-*p* states are fully empty. This gives a semimetal for Sb at ambient conditions. The DoS presented in Fig. 3 contains the features expected from a semimetal: the Fermi level is at the bottom of the valley separating the bonding and antibonding states, the value of DoS at E_F, N_F, is very small, 0.269 states/Ryd, and the energy gap is zero. A final observation from Fig. 2 is that the amount of overlap between the *s* and *p* states gets larger at smaller atomic volumes. This way structures with higher coordination become more favorable as pressure is increased.

Development of the DoS with increasing compression, starting from zero-pressure, Fig. 3, can be followed by the

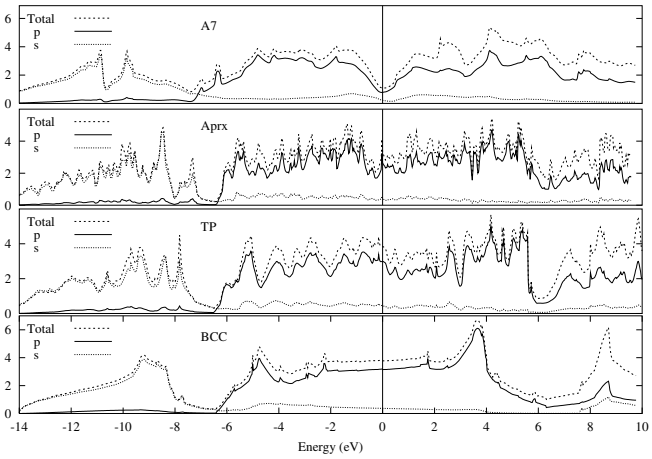

Fig. 4. Density of states computed for all structures considered at a volume where Sb-II is stable.

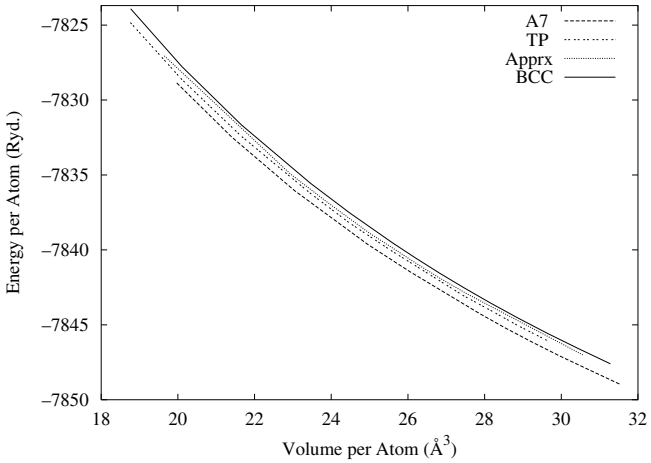

Fig. 6. Comparison of eigenvalue sums for core plus valence states as a function of atomic volume.

help of Fig. 4 and Fig. 5. For each structure densities of states are computed at two different volumes: at a volume of ~ 23 Å^3, where Sb-II phase is stable, Fig. 4, and at ~ 20 Å^3, where BCC phase is stable, Fig. 5. As pressure is applied, N_F is seen to increase from its near-zero value implying transition to metallicity. In Fig. 3 the region dominated by *s* states (between ~ -10 and -5.5 eV) is sharply separated from the *p*-dominated region (between ~ -5.5 and 7 eV). For all investigated crystal structures this sharp separation persists at higher pressures as evidenced by the DoS curves of Fig. 4 and Fig. 5 and the amount of the *p* (*s*) contribution in the *s*-dominated (*p*-dominated) region increases with decreasing volume. These observations imply that the *s*-*p* overlaps slowly enhance with increasing compression; but the system has certainly not reached the point of crossing into a nearly free-electron-like regime. So, even in the BCC phase *s* orbitals and *p* orbitals are sufficiently isolated to sustain the sharp separation. Another feature common to all considered structures is the growing bandwidths with increasing pressures. Therefore, even the *wrong* crystal structure shows the same basic features of the DoS. More importantly, the similarity between the DoS curves of the approximant and the TP structure contrasts sharply the large difference in total energy.

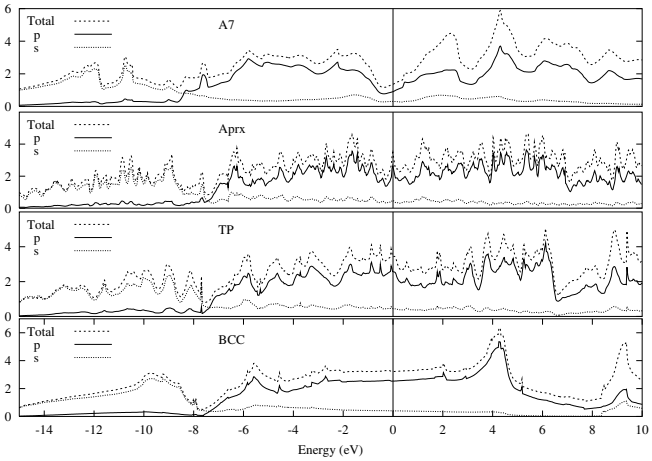

Fig. 5. Density of states computed for all structures considered at a volume where BCC is stable.

It is worthwhile to discuss especially this issue in some detail since in some investigations the total energy is decomposed and only the magnitude of a single contribution is taken into account for discussing the stability of a certain crystal structure in comparison to alternative atomic arrangements [13, 14]. The most relevant component in this type of approaches is the band energy, defined as the sum of the energies of the occupied states: $E_{\text{band}} = \int^{E_F} D(E)\, E\, \mathrm{d}E$, where $D(E)$ is the density of states. Obviously, this quantity will be of little use whenever the DoS of the structures under consideration are very similar. In the case of Sb, this is exactly what happens regarding the approximant and the TP structure. It is impossible to discriminate between these two structures based solely on E_{band} or other concepts derived from E_{band}. Fig. 6 shows how eigenvalue sums (core plus valence) vary as a function of atomic volume for all structures. The behaviour of the approximant (favored structure) and the TP structure (unfavored) are very similar, they both assume an intermediate position between the A7 and BCC structures. On the other hand, the actual fundamental quantity, total energy, naturally differentiates between these two in a very clear way! This particular case is a good example showing that decomposing the total energy to justify or reject a proposed crystal structure is not a reliable approach. Yet, one still feels a need to go beyond the total energy in order to arrive at a deeper understanding of chemical bonding properties. The ELF can be helpful in this context by providing information on, e.g., covalent interactions.

We will refer to the atoms forming the chains that run along the sides (the center) of the body-centered tetragonal sublattice as 'corner' ('center') guest atoms (see Fig. 1). In Fig. 7(a) and Fig. 7(b) contour plots of the ELF along the chains of the 'corner' guest atoms in the approximant and the TP structure, respectively, are shown. The chains run horizontally at the centers of the figures. The remaining structures are due to the contributions of the nearby host atoms none of which lying in the plane of the figure. Between the guest atoms of the approximant there are ELF attractors of value 0.5 indicating guest-guest bonding along the chains. This bonding between the guest atoms in the approximant contributes binding energy thus lowering

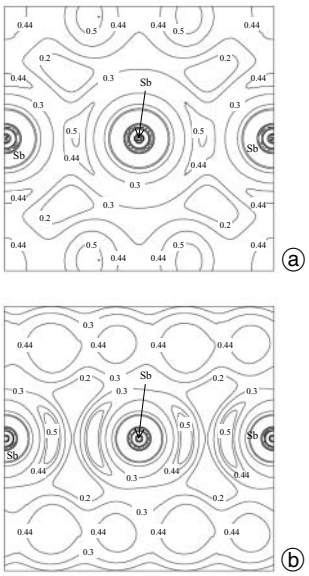

Fig. 7. ELF contour plot (**a**) along the 'corner' chains in the approximant, (**b**) along the 'corner' chains in the TP structure. The chains run horizontally along the center.

the total energy. In the TP structure, however, there are no ELF maxima between the guest atoms, and consequently, the lack of guest-guest bonding in the TP structure results in a higher total energy. In this sense, ELF-based analyses emerge as tools complementary to DoS-based approaches.

The case of 'center' chains in the approximant deserves a closer look. The ELF contour plot is shown in Fig. 8. Although the spacing between all guest atoms is uniform, the ELF contours in Fig. 8 are clearly asymmetrical. In fact, the values of the ELF attractors are 0.561 and 0.442 for the pair on the left and on the right, respectively. The integration of the charge density in the basin with attractor value 0.561 gives 1.98 electrons while the other basin holds only 0.42 electrons. In contrast, the ELF analysis of the 'corner' chains (Fig. 7(a)) does not yield such an asymmetry; there, the ELF attractor values are the same between all pairs. The chains of the TP structure do not have such an asymmetry.

The difference in the behaviours of the 'corner' and the 'center' chains in the approximant stems from the location of host layers. This can be seen by the help of Fig. 9, which shows a projection of Fig. 1 onto the (x, z) plane. For any 'corner' guest atom, its nearest guest-neighbors on either side have an identical environment, and this

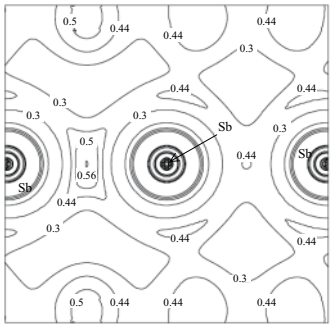

Fig. 8. ELF contour plot along the chain of 'center' guest atoms in the approximant. The chain runs horizontally along the center.

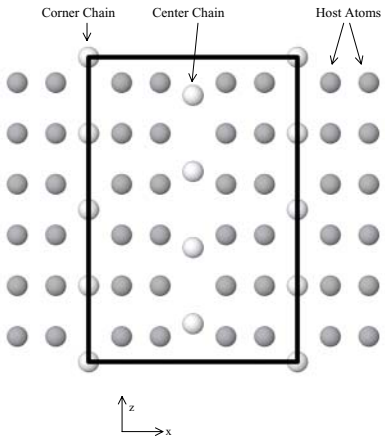

Fig. 9. The projection of crystal structure of the approximant onto the (x, z) plane.

gives the same ELF attractor value for all pairs along 'corner' chains. On the other hand, for a 'center' guest atom the regions between the neighbors on opposite sides are clearly different. On one side there is a single host layer (which is coplanar with a 'corner' layer) sandwiched between the neighbors, whereas on the other side there are two. In the former situation the host atoms are sufficiently away from the 'center' guest atoms, there is no bonding between these host atoms and the 'center' guest atoms. In the latter case, each 'center' guest atom has four host atoms as near neighbors and with each it forms two-center bonds. Due to this asymmetrical environment, the ELF attractor values and the number of electrons contained in the basins turn out to be different on the opposite sides of a 'center' guest atom.

In summary, the amount of *s-p* mixing increases with increasing pressure, and structures with higher coordination become possible. The Sb-II modification consists of two substructures in the form of a modulated incommensurate host-guest arrangement. The relatively high total energy of the structure suggested earlier [18] for the Sb-II phase is explained by the lack of guest-guest binding in that structure. The Sb-II phase is followed by the BCC phase, for which the calculated DoS still shows a structured shape, indicating that the *s-p* mixing has not yet reached the level of a nearly free-electron-like behaviour.

References

[1] Schwarz, U.: Metallic high-pressure modifications of main group elements. Z. Kristallogr., **219** (2004) 376–390.

[2] Mujica, A.; Rubio A.; Muñoz, A.; Needs, R. J.: High-pressure phases of group-IV, III–V, and II–VI compounds. Rev. Mod. Phys. **75** (2003) 863–912.

[3] Schwarz, U.; Takemura, K.; Hanfland, M.; Syassen, K.: Crystal structure of cesium-V. Phys. Rev. Lett. **81** (1998) 2711–2714; Hanfland, M.; Schwarz, U.; Syassen, K.; Takemura, K.: Crystal structure of the high-pressure phase silicon VI. Phys. Rev. Lett. **82** (1999) 1197–1200; Takemura, K.; Christensen, N. E.; Novikov, D. L.; Syassen, K.; Schwarz, U.; Hanfland, M.: Phase stability of highly compressed cesium. Phys. Rev. B**61** (2000) 14399–14404; Hanfland, M.; Syassen, K.; Christensen, N. E.; Novikov, D. L.: New high-pressure phases of lithium. Nature **408** (2000) 174–178; Hanfland, M.; Loa, I.; Syassen, K.: Sodium under pressure: bcc to fcc structural transition and pressure-volume relation to 100 GPa. Phys. Rev. B**65** (2002) 184–109.

[4] McMahon, M. I.; Degtyareva, O.; Nelmes, R. J.: Ba-IV-type incommensurate crystal structure in Group-V metals. Phys. Rev. Lett. **85** (2000) 4896–4899.

[5] McMahon, M. I.; Rekhi, S.; Nelmes, R. J.: Pressure dependent incommensuration in Rb-IV. Phys. Rev. Lett. **87** (2001) 055501.
[6] McMahon, M. I.; Nelmes, R. J.; Rekhi, S.: Complex crystal structure of cesium-III. Phys. Rev. Lett. **87** (2001) 255502.
[7] Nelmes, R. J.; McMahon, M. I.; Loveday, J. S.; Rekhi, S.: Structure of Rb-III: Novel modulated stacking structures in alkali metals. Phys. Rev. Lett. **88** (2002) 155503.
[8] Neaton, J. B.; Ashcroft, N. W.: Pairing in dense lithium. Nature **400** (1999) 141–144; Neaton, J. B.; Ashcroft, N. W.: On the constitution of sodium at higher densities. Phys. Rev. Lett. **86** (2001) 2830–2833.
[9] Schwarz, U.; Jepsen, O.; Syassen, K.: Electronic structure and bonding in the Cmca phases of Si and Cs. Solid State Commun. **113** (2000) 643–648.
[10] Reed, S. K.; Ackland, G. J.: Theoretical and computational study of high-pressure structures in barium. Phys. Rev. Lett. **84** (2000) 5580–5583.
[11] Ahuja, R.; Eriksson, O.; Johansson, B.: Theoretical high-pressure studies of Cs metal. Phys. Rev. B**63** (2000) 014102.
[12] Christensen, N. E.; Novikov, D. L.: High-pressure phases of the light alkali metals. Solid State Commun. **119** (2001) 477–490.
[13] Häussermann, U.; Söderberg, K.; Norrestam, R.: Comparative study of the high-pressure behaviour of As, Sb, and Bi. J. Am. Chem. Soc. **124** (2002) 15359–15367.
[14] Häussermann, U.: High-pressure structural trends of Group 15 elements: Simple packed structures versus complex host – guest arrangements. Chem. Eur. J. **9** (2003) 1471–1478.
[15] Schwarz, U.; Akselrud, L.; Rosner, H.; Ormeci, A.; Grin, Yu.; Hanfland, M.: Structure and stability of the modulated phase Sb-II. Phys. Rev. B**67** (2003) 214101.
[16] Aoki, K.; Fujiwara, S.; Kusabe, M.: New phase transition into the bcc structure in antimony at high pressure. Solid State Commun. **45** (1983) 161–163.
[17] Vereschchagin, L. F.; Kabalkina, S. S.: Phase transitions in antimony at high pressures. Sov. Phys. JETP **20** (1965) 274; Kolobyanina, T. N.; Kabalkina, S. S.; Vereschchagin, L. F.; Fedina, L. V.: Investigation of crystal structure of antimony at high pressures. Sov. Phys. JETP **28** (1969) 88; Duggin, M. J.: High-pressure phase in arsenic and its relation to pressure-induced phase changes in group 5B elements. J. Phys. Chem. Solids **33** (1972) 1267.
[18] Iwasaki, H.; Kikegawa, T.: Crystal structure of the high pressure phase of antimony SbII. High Pressure Res. **6** (1990) 121–132.
[19] Wills, J. M. (unpublished); Wills, J. M.; Cooper, B. R.: Synthesis of band and model Hamiltonian theory for hybridizing cerium systems. Phys. Rev. B**36** (1987) 3809–3823; Price, D. L.; Cooper, B. R.: Total energies and bonding for crystallographic structures in titanium-carbon and tungsten-carbon systems. Phys. Rev. B **39** (1989) 4945–4957; Wills, J. M.; Eriksson, O.; Alouani, M.: Full-potential LMTO total energy and force calculations. In: (Ed. H. Dreysse), *Electronic Structure and Physical Properties of Solids: The Uses of the LMTO Method*. Springer, Berlin, 2000, p. 148.
[20] Koepernik, K.; Eschrig, H.: Full-potential nonorthogonal local-orbital minimum-basis band-structure scheme. Phys. Rev. B **59** (1999) 1743–1757.
[21] Andersen, O. K.: Linear methods in band theory. Phys. Rev. B **12** (1975) 3060–3083; Andersen, O. K.; Jepsen, O.: Explicit, first-principles tight-binding theory. Phys. Rev. Lett. **53** (1984) 2571–2574.
[22] Jepsen, O.; Andersen, O. K.: The Stuttgart TB-LMTO-ASA program, version 4.7, Max-Planck-Institut für Festkörperforschung, Stuttgart, Germany, 2000.
[23] Becke, A. D.; Edgecombe, K. E.: A simple measure of electron localization in atomic and molecular systems. J. Chem. Phys. **92** (1990) 5397–5403.
[24] Savin, A.; Jepsen, O.; Flad, J.; Andersen, O. K.; Preuss, H.; Schnering, H. G. v.: Electron localization in solid-state structures of the elements: the diamond structure. Angew. Chem. Int. Ed. **31** (1992) 187–188.
[25] This is the same approximant as was used previously in Ref. [15].
[26] Kohn, W.; Sham, L. J.: Self-consistent equations including exchange and correlation effects. Phys. Rev. **140** (1965) A1133–A1138.
[27] Hohenberg, P.; Kohn, W.: Inhomogeneous electron gas. Phys. Rev. **136** (1964) B864–B871.
[28] Savin, A.; Nesper, R.; Wengert, S.; Fässler, T. F.: ELF: The electron localization function. Angew. Chem. Int. Ed. Engl. **36** (1997) 1808–1832.
[29] Silvi, B.; Savin, A.: Classification of chemical bonds based on topological analysis of electron localization functions. Nature **371** (1994) 683–686.
[30] Savin, A.; Silvi, B.; Colonna, F.: Topological analysis of the electron localization function applied to delocalized bonds. Can. J. Chem. **74** (1996) 1088–1096.
[31] Kohout, M.; Wagner, F. R.; Grin, Yu.: Electron localization function for transition-metal compounds. Theor. Chem. Acc. **108** (2002) 150–156.
[32] Kohout, M.: Program Basin, version 2.4, Max-Planck-Institut für Chemische Physik fester Stoffe, Dresden, Germany, 2003.
[33] Skriver, H. L.: The LMTO Method, Springer, Berlin, 1984; p. 25–27.
[34] Since the Wigner-Seitz rule is based only on the logarithmic derivative of the partial wave, it ignores the effects of hybridization.